Hot-roll Fabrication of Anisotropic Nanograin Nd-Fe-B Magnet

Chaochao Pan[1,2,3], Gaoyuan Ouyang[1,2], Wei Tang[1,2], Xubo Liu[1,2], Ryan Ott[1,2], Ikenna Nlebedim[1,2], Eunjeong Kim[1,4], Scott K. McCall[1,4], Alexander A. Baker[1,4], Jun Cui[1,2,3*]

1. Critical Material Institute, Ames, Iowa, 50011, USA
2. Ames National Laboratory, Ames, Iowa, 50011, USA
3. Iowa State University, Ames, Iowa, 50011, USA
4. Lawrence Livermore National Laboratory, Livermore, CA, 94550, USA

* Author for correspondence: cuijun@iastate.edu

Abstract

Nd-Fe-B based magnets have the highest energy product among all permanent magnets, which is required for numerous clean energy technologies. For higher temperature applications (T > 150 °C), additions of heavy rare earth elements (HREEs) such as Dy are required to maintain sufficient coercivity during operation. Additions of Dy are expensive, and thus, it is desirable to reduce the need for HREEs by reducing the grain size to the nanoscale, which increases the coercivity and decreases its temperature dependence. Here, we report a novel nanograin Nd-Fe-B magnet fabrication method that is continuous and low-cost. The process uses mechanically milled Nd-Fe-B melt-spun flakes as feedstock powder that is packed into a metal vessel and then hot-rolled to form a fully dense and highly textured strip magnet with tailored thicknesses, down to 800 µm. Using this process, fully dense nanograin bulk magnets can be synthesized in minutes compared to the traditional multi-step processes that are typically low throughput.

Introduction

Nd-Fe-B "Neo" based permanent magnets are the preferred magnet for many applications requiring high energy efficiency and high power density. The most powerful commercial Neo magnet can reach 55 MGOe (440 kJ/m^3) at room temperature.[1] The excellent hard magnetic properties in the $Nd_2Fe_{14}B$ intermetallic phase arise from the high magnetocrystalline anisotropy attributed to the spin-orbit coupling and crystal-field interactions from 4f electrons.[2] The phase has a primitive tetragonal unit cell containing 68 atoms and is intrinsically brittle due to its mixed metallic-covalent bonding and limited slip systems for dislocations to glide. Manufacturing defects such as non-uniform microstructures and residual stress further reduce their ability to impede crack propagation. The fracture toughness of commercial Neo magnet is about 3.9-5.5 MPa$\sqrt{\mathrm{m}}$.[3,4] Even with extra caution, manufacturers often see more than 20% failure rate when machining parts with a high aspect ratio. As the size of the magnets used in some technologies approaches to sub-millimeter scale, the loss of materials due to high machining failure rate has a profound effect on critical materials usage and manufacturing costs. Failures during machining result in large increases in embodied energy and costs since the “scrap” recycling is energy and cost intensive. Another challenge with thin magnets is the variability in magnetic properties from part to part. Small variations in structures/compositions in large sintered blocks become more pronounced when processed into thin geometries, partially caused by the temperature gradient during heat treatment.

Near-net-shape (NNS) manufacturing of small magnets via sintering is difficult due to the significant shrinkage (~25%). Processes such as additive manufacturing, injection molding, and hot deformation have been shown as potential NNS processes[5]. However, these routes have low throughput and high cost. For example, additive manufacturing is not well-suited for producing fully dense anisotropic Neo magnets as there is limited control of grain size, texture, and grain boundary phases during manufacturing. Bonded magnets are ideally suited for NNS manufacturing as the materials can be processed at relatively low temperatures (170-300 ^{o}C) depending on the binder and molding technique.[6] Bonded magnets exhibit excellent damage tolerance. However, they contain 10-50 vol. % of binder, which limits the magnetization and are typically isotropic. The best commercial bonded neo magnet exhibits 20 MGOe at room temperature, less than half of a mid-grade sintered Neo magnet.[7]

Hot press followed by hot deformation is the most straightforward NNS method for producing fully dense, high-energy product magnets with cross-section close to or matching the final dimensions. The process uses nano-grained powder milled from melt-spun ribbons as feedstock. This powder is hot pressed for densification, then subjected to another hot deformation step to achieve preferred texturing. The hot pressing step is carried out at 700-750 °C so that a liquid grain-boundary phase (T_{melt} ~ 670 °C) can aid the densification.[8] The subsequent hot deformation step produces texture at 700-800 °C via preferred grain growth. A common hot deformation method is die-upsetting of the hot-pressed precursors, which results in anisotropic structures with the c-axis parallel to the pressing direction.[9] Another example is the production of radially oriented ring magnets by backward extrusion.[10,11] The shortcomings are the cost of the two-step process and limited part size and shape. More importantly, these are batch processes requiring prolonged application of stress, heat, and inert environment or vacuum.

The newly developed hot rolling approach directly addresses these shortcomings by combining hot press densification and hot deformation texture development into one continuous process. The powders are packed and sealed into a stainless steel (SS) tube (could be in other forms such as a pouch or box, and using other metals such as copper, bronze, brass, and non-magnetic steel) and then hot-rolled to a ~70% thickness reduction at the designed temperature. The SS tube serves as a vacuum enclosure and mold, eliminating the need for a vacuum furnace. It also eliminates the loading-unloading processes, hence enabling continuous production of strip magnets. The thickness of the strip magnet can be controlled through the initial tube diameter. Another issue with the conventional hot pressing hot deformation process is the difficulty of controlling grain growth when exposing the material to high temperatures and high stress needed for texture development. The newly developed hot rolling method addresses this issue by reducing the time exposed to high temperatures. The heating and cooling are rapid because the thermal mass is small, the tube is in direct contact with the cold roller, and there is no heavy die and the de-die process. Moreover, the materials could be heated by a simple induction coil, allowing rapid temperature ramping in just a few seconds instead of waiting for the whole tube to heat up in a furnace. Fig. 1 compares the novel hot-roll process with the traditional hot-press hot-roll process for making nanograin anisotropic Neo magnets.

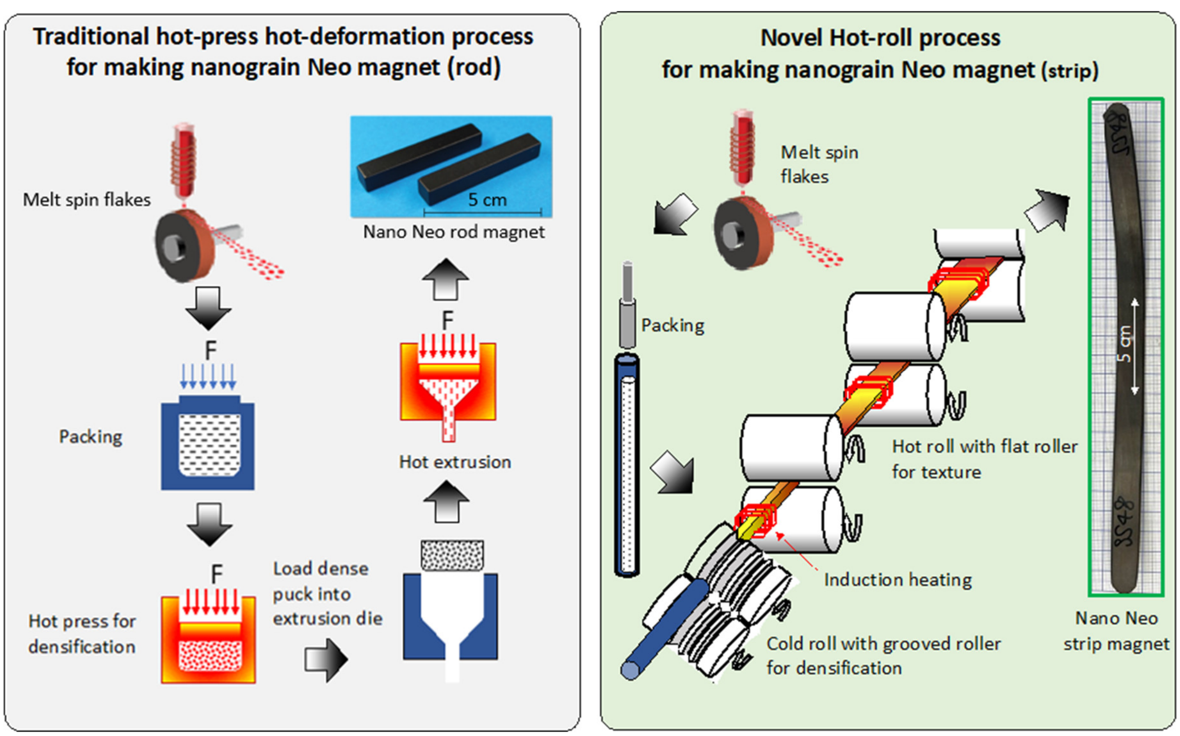

Fig. 1. Manufacturing processes for making an anisotropic NdFeB nanograin magnet: the traditional hot-press hot-deformation process (left) and the novel hot-roll process (right).

The newly developed hot rolling process is designed for producing nanograin magnets, whose coercivity is less sensitive to temperature than the sintered magnet. With the grain size reduced to the size of a single magnetic domain, the domain reversal is delayed due to the increased grain boundary pinning, which enhances the coercivity. This is the only known engineering approach with the potential to replace the HREE approach for making the Neo magnet work at high temperatures.

Materials and experiments

The raw Nd-Fe-B flakes (MQU-F) used in this study were acquired from Magnequench Co. Ltd. This commercial powder is available in the form of melt-spun flakes. The nominal composition is $Nd_{13.9}Fe_{75.6}Ga_{0.5}Co_{4.5}B_{5.6}$ (at.%). The flakes were ground using mortar and pestle and passed through a mesh sieve with $\leqslant$ 355 µm in an Ar environment. The powder was then packed into a stainless steel tube (SS 316) with the open end welded shut in vacuum. The outside diameter of the tube was 12.7 mm and the wall thickness was 1.65 mm.

The powder-packed tube (circular cross-section) was first cold rolled/shaped into a square tube with ~66% cross-section area reduction using grooved rollers. The obtained square tube was placed in a box furnace preheated to 780 °C. After 2-5 min, the tube was pulled out from the furnace and inserted into a flat roller with preset gap thickness. Note that the roller itself was not heated. This process was repeated multiple times to achieve the desired overall thickness reduction. The heating dwelling time was 5 min for the first pass, and gradually reduced to 2 min for the rest passes.

The M-H curves of the sample were measured with a Vibrating Sample Magnetometer (VSM, PPMS, Quantum Design Inc) at 9 T. The specimens (3 x 3 x 2 mm^3) were cut from the hot rolled strip by electric discharge machining (EDM), and the M-H curves were measured normal to the rolling plane and along the rolling direction. The density of the hot rolled sample was measured by Archimedes method. The texture of the samples was measured using an X-ray diffractometer (PANalytical X'Pert) equipped with a Co target at a step size of 0.008° 2θ angle. To map out the effects of temperature on the microstructure of feedstock material, the feedstock powders were sealed in quartz tubes backfilled with 1/3 Ar and heat treated from 740 °C to 840 °C for a duration ranging from 2 min to 30 min, followed by water quenching.

The cross-sectional microstructure was observed with an FEI Teneo LoVac field-emission scanning electron microscope (FE-SEM). The surface of the sample was finished with 50 nm AlO_2 suspension fluid.

Results and discussion

Pictures of the tube before and after the processing are shown in Fig. 2. The round tube was shaped into a square tube after the room temperature combination rolling (Fig.2b). This step increases the green body density, which helps with densification when the sample is heated and rolled. The strain-hardened edges of the square tube act as boundary conditions to allow for more efficient stress application on the powders. The density of the sample after the combination rolling, Fig 2(b), was 4.7 g/cm^3. After hot rolling, the SS tube was deformed to strip, as shown in Fig. 2c. The total thickness reduction of the powder compact was ~70%. Nd-Fe-B strip with a thickness of 0.8-3 mm can be obtained by peeling off the SS casing. The thin SS layers (about 10% of the overall thickness) can be kept as part of the magnet protection layer.

Fig. 2. Photo showing the powder-packed stainless steel tube sample in different processing steps. (a) after filling and sealing; (b) after combination cold rolling; (c) after hot rolling. The grid spacing is 10 mm.

The room temperature M-H curves of a hot-rolled sample (corrected by the demagnetization factor) and the as-received ribbon powder are shown in Fig. 3. The as-received powders are isotropic, and thus, exhibited a relatively low $(BH)_{max}$ of 11.3 MGOe. The sample hot-rolled 4 times at 780 °C exhibited an energy product $(BH)_{max}$ of 37.6 MGOe. The remanence and squareness of the M-H loop are significantly improved, indicating strong texturing in the hot-rolled samples. The hot-rolling process sacrificed some coercivity of the as-received powder, but significantly improved the remanence (B_r) and squareness of the curve, leading to greatly increased energy product. The density of the magnet was 7.38 g/cc, which is equivalent to 97.1% densification (the full density is 7.6 g/cc). It shows that the hot-rolling process is effectively in achieving high density and strong texture simultaneously.

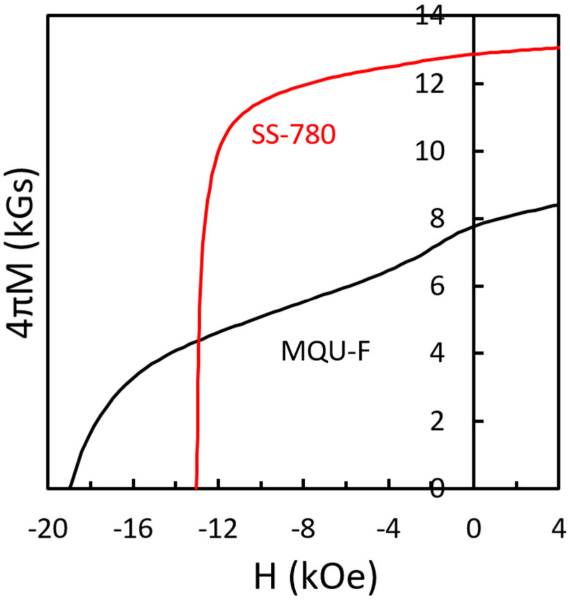

Rolling Temperature (°C)	780
H_{cj} (kOe)	13.01
M_r/M_s (%)	87.70
Density (g/cc)	7.38 (97.1%)
$(BH)_{max}$ (MGOe)	37.64

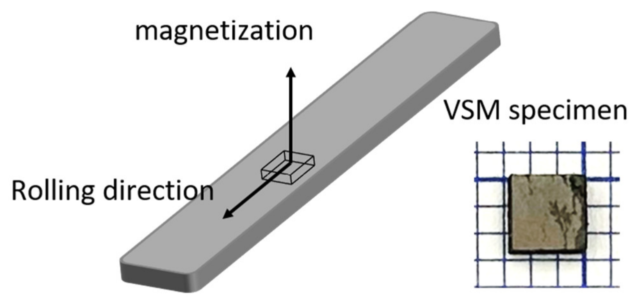

Fig. 3. Room temperature M-H curves of powders and hot rolled samples, their magnetic properties, schematics of the strip, and the picture of the sample.

Microstructures of the hot-rolled sample are shown in Fig. 4. It consists of two types of grains, the equiaxial grains and the elongated grains (Fig. 4(b)). The grain size analysis of the two types of grains is presented in Fig. 5. About 500 grains of each type were measured by linear intercept method. The average size of the equiaxial grains was around 260 nm, while the average width of the elongated grains was only 40 nm. This large difference in grain sizes was due to the differences in cooling rates between the sides of the ribbon that was in contact with the melt-spinning wheel (wheel side) and the side that was not (the free side). The free side of the ribbons experienced slower cooling rates which resulted in larger grain sizes, as seen in Fig. 4(a). The powder particles deformed under the rolling stress, however the coarse grains remained equiaxed after rolling, which inhibited grain alignment and texture development. In contrast, the nano-scale equiaxed grains from the wheel side of the as-received ribbon powder became elongated platelets primarily aligned parallel to the rolling direction (Fig. 4(c)). The average angle of the grains deviating from the rolling direction was about 12.5° ± 0.4°. The exact mechanism for texture development during the thermal-mechanical process is still under debate. The two prevailing theories are the grain boundary sliding[12,13] and the liquid diffusion models[14]. The grain boundary sliding model attributes the grain alignment to the rotation and sliding of the grains under the external stress with the assistance of the liquid grain boundary phase at the deformation temperature. The argument is that the extent of grain alignment increases with the deformation ratio. On the other hand, the liquid diffusion model claims that the 2-14-1 phase diffuses from unfavored grains whose c-axis are misaligned with the compressive stress to the favored ones whose c-axis are parallel with the compressive stress through the liquid grain boundary phase. The driving force of the diffusion is the elastic energy minimization due to the elastic anisotropy between the a-axis and the c-axis.

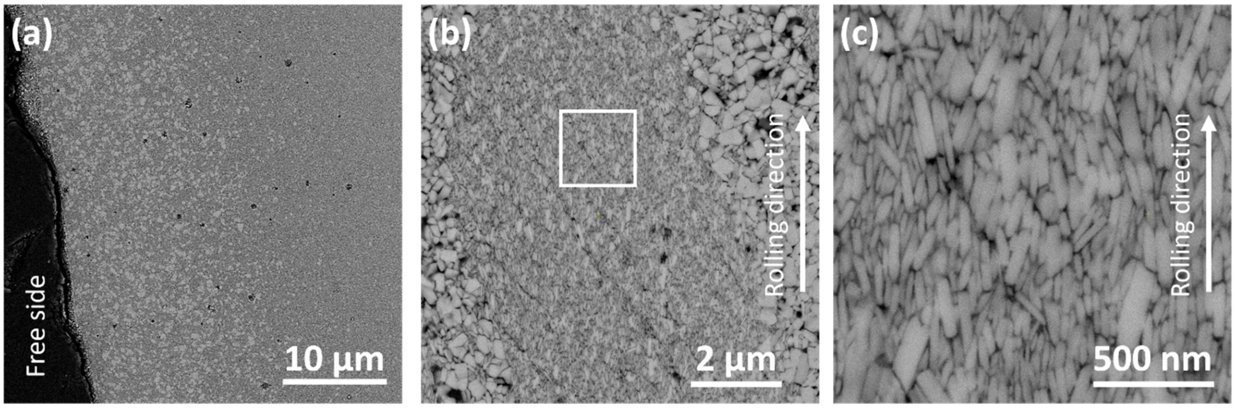

Fig. 4. SEM image of (a) as-received feedstock MQU-F powder, (b) hot-rolled magnet showing powder boundary, and (c) hot-rolled magnet showing aligned grains.

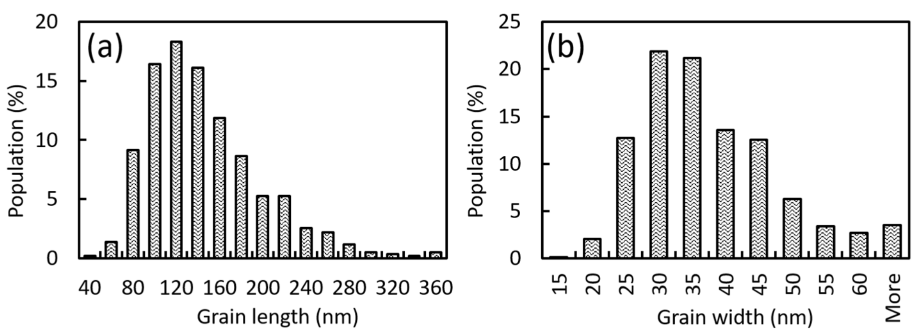

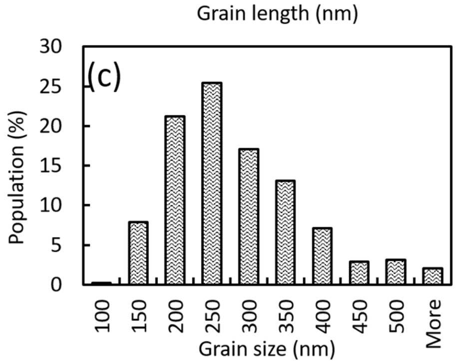

(d)	Equiaxial grain	Elongated grain
Size (nm)	259.7 ± 4.3	/
Length (nm)	/	135.8 ± 2.2
Width (nm)	/	35.5 ± 0.5
Orientation (°)	/	12.5 ± 0.4
Aspect ratio	~1	3.96 ± 0.06

Fig. 5. The distribution of (a) the length of the elongated grains, (b) the width of the elongated grains, and (c) the size of the equiaxial grains. (d) The statistics of both types of grains. The orientation angle stands for the angle between the rolling direction and the long axis of the elongated grain.

To characterize the texture of the hot-rolled sample, XRD measurements were conducted along the out-of-plane direction and the rolling direction (Fig. 6). $Nd_2Fe_{14}B$ has a tetragonal crystal structure (tP68), with its c-axis being the magnetic easy axis. The rolling stress direction is normal to the rolling direction, and thus, it is the direction where the c-axis is preferentially aligned. When measured in the out-of-plane direction, the relative intensities of the planes parallel to the c-axis ((004), (006), and (105) peaks) are stronger than those of the feedstock powder (Fig. 6). And when measured along the in-plane direction, there is an increase in relative intensities of the basal plane (601) and (410). These patterns suggest a highly textured sample with the c-axis aligned out-of-plane, consistent with the magnetic measurement results.

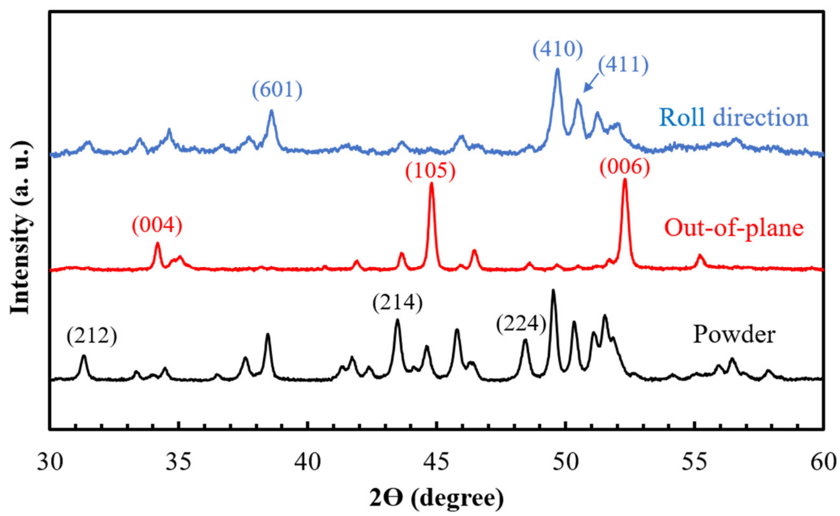

Fig. 6. X-ray diffraction patterns of the feedstock powders and the hot-rolled samples were measured in the out-of-plane and rolling directions.

The temperature dependence of the magnetic properties of the hot-rolled sample was measured along with the feedstock powder MQU-F and a N45 sintered magnet[1] (containing zero Dy), and the results are shown in Fig. 7. Due to the limitation of our measurement system, only the data from room temperature to 400 K (127 °C) were available. It shows the hot-rolled magnet has better α (temperature coefficient of B_r) but inferior β (temperature coefficient of H_{cj}) to the N45 grade sintered magnet for the temperature range that was measured. However, with rising temperature, the β of the hot-rolled magnet improved while the β of the N45 magnet deteriorated. At 400 K (127 °C) they crossed. This trend is likely to continue, implying that the hot-rolled magnet will exhibit better β at higher temperatures than the N45 sintered magnet.

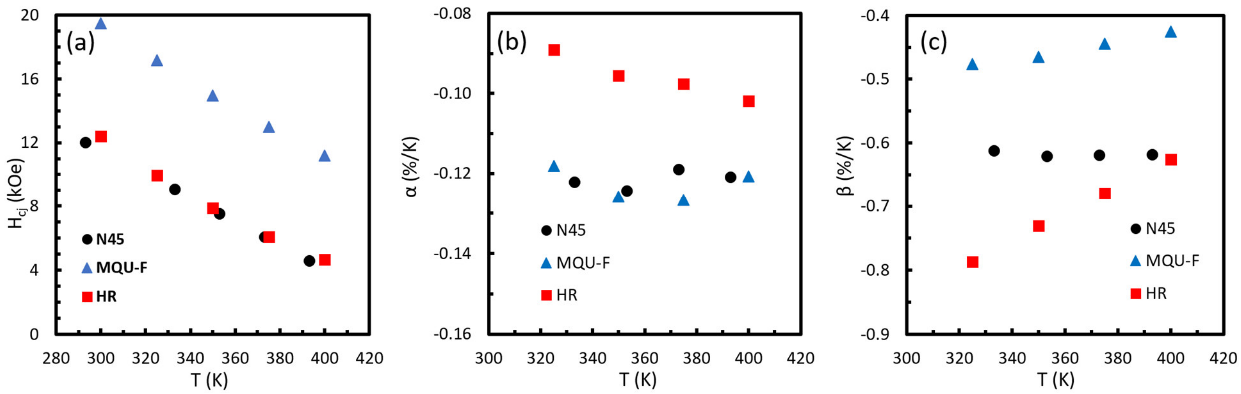

Fig. 7. Comparison of the temperature dependence of the hot-rolled strip magnet (labeled as HR), feedstock powder MQU-F, and typical N45 sintered magnet: (a) coercivity, (b) remanence magnetization α, and (c) coercivity β.

The parameters for the hot-rolling process include rolling temperatures, stress, total thickness reduction, reduction per pass, number of passes, casing material, roller size, speed, etc. The effects of these parameters on microstructures are often coupled, requiring extensive experiments to optimize. In this article, due to the length limit, we will only report the result of our study on rolling temperatures, with the rest of the processing parameters fixed.

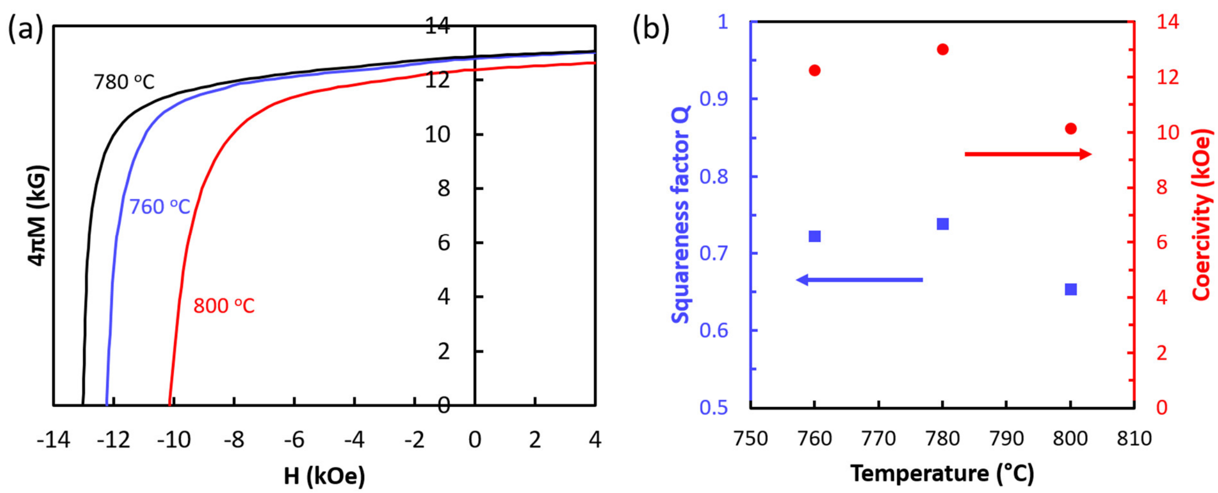

Fig. 8. The effect of rolling temperature on magnetic properties. (a) the demagnetization curve, and (b) the squareness factor and coercivity.

In the traditional hot-press hot-deformation process, there is a compromise between the coercivity and squareness of M-H curves.[12] The increase in deformation temperature facilitates grain rotation and texture development but also negatively affects coercivity by encouraging grain growth. This dilemma may not be entirely applicable to the hot-roll process. Fig. 8 illustrates the effect of rolling temperatures on the magnetic properties. The intermediate rolling temperature of 780 °C achieves the highest coercivity and squareness factor Q (defined as the ratio of the knee field (H_k, the field when magnetization is 90% of the remanence) and coercivity H_c). While heavier grain growth at higher temperatures can explain why the coercivity (10.2 kOe) at 800 °C is the lowest, it cannot explain why the coercivity for the magnet rolled at 760 °C (12.3 kOe) is lower than the one at 780 °C (13.0 kOe). A possible explanation can be formulated after considering the effect of stress on grain growth.[15] Our hot roller is strain-controlled. Once its gap is set, the processing load will be self-adjusted depending on the stiffness of the sample. The sample processed at a lower temperature will have higher stiffness and, thereby, will experience higher stress. At 760 °C, the contribution to the grain growth from the increase of load due to higher stiffness may overwhelm the saving from the decrease of temperature, leading to the unexpected grain growth and the consequent coercivity drop. In addition, the powder annealing study (Fig. 9) reveals that abnormal grain growth initiates at 800 °C. The abnormal grains are equiaxial, so they do not have preferential alignment during the deformation. This abnormal grain growth leads to worse texture than samples processed at lower temperatures, despite the grains being easier to rotate.

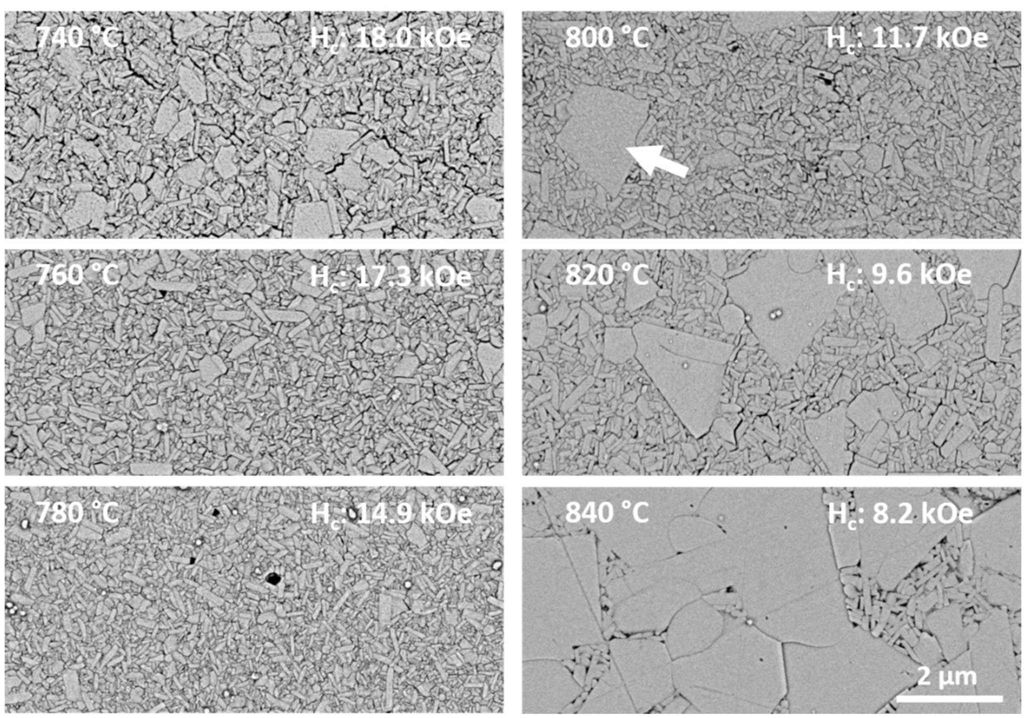

Fig. 9. The microstructure and coercivity of MQU-F powder after 15 min of annealing at temperatures between 740 to 840 °C. The arrow indicates the onset of abnormal grain growth.

Conclusion

A hot rolling process for near-net-shape fabrication of anisotropic nanograin Nd-Fe-B magnets is developed. Compared to the existing processing routes for making Nd-Fe-B magnets, the newly developed hot rolling method has several advantages: 1) the continuous manufacturing nature of the hot-rolling process dramatically improves productivity; 2) The elimination of the vacuum furnace reduces capital cost and enables fast heating and cooling in ambient air, making it easy for the industry to adopt the technology; 3) the metal casing provides mechanical and anti-corrosion protection to the magnets; 4) the near-net-shape manufacturing minimizes machining cost and material waste; 5) induction heating reduces the heating time and potentially increase coercivity; 6) Since the magnet along the rolling direction experiences exactly the same thermal and mechanical history, the property of the entire strip is assumed to be consistent, in contrast to the thermal gradient induced variation for sintered block magnets; 7) The strip magnets can be readily curved to meet the geometric requirement in electrical machines.

Acknowledgment

This work is supported by the Critical Materials Innovation Hub (CMI), funded by the U.S. Department of Energy (DOE), Office of Energy Efficiency and Renewable Energy, Advanced Materials and Manufacturing Technologies Office (AMMTO). The work was performed in Ames National Laboratory, operated for the U.S. Department of Energy by Iowa State University of Science and Technology under Contract No. DE-AC02-07CH11358. Portions of this work was performed under the auspices of the U.S. Department of Energy by Lawrence Livermore National Laboratory under Contract DE-AC52-07NA27344.

Conflict of Interest

The authors declare that they have no conflict of interest.

References

[1] https://www.arnoldmagnetics.com/products/neodymium-iron-boron-magnets/

[2] Skomski, R., and D. J. Sellmyer. "Anisotropy of rare-earth magnets." *Journal of Rare Earths* 27.4 (**2009**): 675-679.

[3] Horton, J. A., J. L. Wright, and J. W. Herchenroeder. "Fracture toughness of commercial magnets." *IEEE Transactions on Magnetics* 32.5 (**1996**): 4374-4376.

[4] Li, Wei, Anhua Li, and Huijie Wang. "Anisotropic fracture behavior of sintered rare-earth permanent magnets." *IEEE transactions on magnetics* 41.8 (**2005**): 2339-2342.

[5] Cui, Jun, et al. "Manufacturing processes for permanent magnets: part II—bonding and emerging methods." *JOM* 74.6 (**2022**): 2492-2506.

[6] Nlebedim, I. C., et al. "Studies on in situ magnetic alignment of bonded anisotropic Nd-Fe-B alloy powders." *Journal of Magnetism and Magnetic Materials* 422 (**2017**): 168-173.

[7] https://mqitechnology.com/products/bonded-neo-powder/

[8] Knoch, K., Bernd Reinsch, and Günter Petzow. "Nd, Fe, B-Its Region of Primary Solidification." *International Journal of Materials Research* 85.5 (**1994**): 350-354.

[9] Mishra, Raja K. "Microstructure of hot‐pressed and die‐upset NdFeB magnets." *Journal of applied physics* 62.3 (**1987**): 967-971.

[10] Croat, John J. "Current status of rapidly solidified Nd-Fe-B permanent magnets." *IEEE Transactions on Magnetics* 25.5 (**1989**): 3550-3554.

[11] Grünberger, W., et al. "Hot deformation of nanocrystalline Nd-Fe-B alloys." *Journal of Alloys and Compounds* 257.1-2 (**1997**): 293-301.

[12] Shioi, Ryosuke, Hiroshi Miyawaki, and Toshiyuki Morita. "Orientation mechanism of hot deformed anisotropic RE-Fe-B magnets." *Denkiseiko* 82.1 (**2011**): 31-37.

[13] Hioki, Keiko. "High performance hot-deformed Nd-Fe-B magnets." *Science and Technology of Advanced Materials* 22.1 (**2021**): 72-84.

[14] Li, Lin, and C. D. Graham. "The origin of crystallographic texture produced during hot deformation in rapidly-quenched NdFeB permanent magnets." *IEEE transactions on magnetics* 28.5 (**1992**): 2130-2132.

[15] Zhang, Yang, Garritt J. Tucker, and Jason R. Trelewicz. "Stress-assisted grain growth in nanocrystalline metals: Grain boundary mediated mechanisms and stabilization through alloying." *Acta Materialia* 131 (**2017**): 39-47.